Chinese Chemical Letters 32 (2021) 2919–2922

Contents lists available at ScienceDirect

Chinese Chemical Letters

journal homepage: www.elsevier.com/locate/cclet

Communication

Hierarchically porous nitrogen-doped carbon foams decorated with zinc nanodots as high-performance sulfur hosts for lithium-sulfur battery

Zhibo Liu[a,b], Li Wang[a,b,*], Wantai Yang[a,b,c]

[a] State Key Laboratory of Chemical Resource Engineering, Beijing University of Chemical Technology, Beijing 100029, China
[b] School of Materials Science and Engineering, Beijing University of Chemical Technology, Beijing 100029, China
[c] Beijing Advanced Innovation Centre for Soft Matter Science and Engineering, Beijing University of Chemical Technology, Beijing 100029, China

ARTICLE INFO

Article history:
Received 14 February 2020
Received in revised form 9 February 2021
Accepted 14 February 2021
Available online 17 February 2021

Keywords:
Nitrogen-doped carbon foams
Hierarchically porous
Lithium-sulfur battery
Zinc nanodots
Hosts

ABSTRACT

To prevent polysulfides from dissolution into electrolyte, we propose a novel and simple approach to nitrogen-doped carbon foams which contain hierarchically porous structure and are decorated with zinc nanodots through one-pot carbonization and activation process. These carbon foams, which serve as hosts for sulfur in lithium battery, can provide a conducting network and shorter diffusion length for Li-ions. Specially, the zinc nanodots derived from the carbothermal reaction of $ZnCl_2$ at high temperature can interact with sulfur/polysulfides by strong chemisorption. In addition, the zinc nanodots can also facilitate the conversion reaction between Li_2S_x ($2 < x < 8$) and Li_2S/Li_2S_2. Therefore, Zn@NCFs/S cathode presents high sulfur utility and large capacity.

The widespread applications of energy storage devices, including wearable electronic devices, electronic vehicles as well as large-scale smart power grids, have stimulated intense research in rechargeable batteries with high energy density [1]. Typically, lithium-sulfur (Li-S) battery uses lithium as an anode and utilizes sulfur as cathode, which performs a high energy density (2600 Wh/kg) based on the reaction: $16Li + 8S = 8Li_2S$. The applications of Li-S battery benefit a lot from sulfur, such as environmental friendliness, low cost and abundant resources [2]. However, there are several problems limiting the development and applications of Li-S battery, including the shuttle effect of polysulfides, non-conductive nature of sulfur, the volume expansion derived from the redox reaction between sulfur and Li_2S and relevant problems from lithium anode [3]. Among the problems that hinder the commercialization of lithium-sulfur battery, polysulfides shuttling is a main factor that leads to self-discharge, lower Coulombic efficiency and severe capacity fading [3].

To overcome the above obstacles, many strategies have been proposed by researchers recently. It is well believed that carbon materials can provide a continuous conductive network during the electronic process. Thus, many carbon materials have been designed in previous work [1,3–5]. However, the connection between polysulfides and the surface of carbon matrix is weak by physical absorption [6], because carbon is intrinsically non-polar while polysulfides are polar. This brings about difficulties in restraining the "shuttling effect". Heteroatom-doped (O, N, P and B) carbon materials have shown certain benefits on the usage of sulfur, which is due to interaction between heteroatom and polysulfides [7–17]. In addition, polysulfides can be prevented from entering electrolyte by modifying carbon with metals or metal oxides such as Co [16], Pd [18], TiO_2 [19–21], Fe_3O_4 [22], SiO_2 [23], MnO_2 [24], $CoFe_2O_4$ [25], SnO_2 [26] and ZnO [6], because of their strong chemical interaction with metal oxides/metals. For example, Lu *et al.* showed that S@Fe_3O_4-NC@ACC had great cycle stability and high capacity due to the introduction of abundant heteroatoms (N, O) and Fe_3O_4 [22]. Zhang *et al.* synthesized a 3D graphene nanosheet-carbon nanotube matrix with cobalt nanoparticles as sulfur host for Li-S battery, which displayed superb cycle ability and rate capacity due to the interaction between polysulfides and metal cobalt [15]. Ma *et al.* developed catalytic palladium nanoparticles loaded on hollow carbon spheres, which had a capacity retention as high as 85% after 100 cycles [17]. However, the electrical conductivity of these carbon materials modified with metal oxides/metals is not satisfactory. Therefore, the key issue is to construct an efficient connection between carbon hosts and metal oxides/metals in order to improve the overall conductivity of cathode.

* Corresponding author at: State Key Laboratory of Chemical Resource Engineering, Beijing University of Chemical Technology, Beijing 100029, China.
E-mail address: lwang@mail.buct.edu.cn (L. Wang).

https://doi.org/10.1016/j.cclet.2021.02.027
1001-8417/

In this work, we report a new approach to manipulate lithium polysulfides conversion *via* strongly coupled Zn and N-doped hierarchically porous carbon foams (Zn@NCFs/S). Starting from poly(acrylamide) (PAM) hydrogel impregnated with $ZnCl_2$, carbonization at a gasification rate of 1 °C/min leads to N-doped hierarchically porous carbon foams. Remarkably, the zinc precursor is not removed after carbonization, but ends up as well-defined zinc nanodots with a loading as high as 7.8 wt% in the hierarchically porous carbon foams (Fig. S1 in Supporting information) [27]. These zinc nanodots can act as efficient catalyst in subsequent electrochemical reaction. Owing to these structural features, sulfur/polysulfides are constrained effectively by the physical absorption from the porous structure and chemisorption from the zinc nanodots and heteroatoms (O, N). Therefore, using Zn@NCFs/S as cathode in Li-S battery can achieve excellent capacity (505 mAh/g, 2 C) after 100 cycles.

The hierarchically porous nitrogen-doped carbon foams decorated with zinc nanodots (Zn@NCFs) were prepared by employing $ZnCl_2$ as chemical activation agent for well-defined hierarchically porous structure (Fig. 1). Acrylamide (AM), which is an outstanding carbon and nitrogen precursor, was mixed with a certain amount of $ZnCl_2$ (0.86 g) in aqueous solution. Subsequent polymerization of AM yielded PAM hydrogels with the zinc precursor inside. Afterwards, the hydrogels were freeze-dried and carbonized at 900 °C at 1 °C/min. Finally, we obtained hierarchically porous nitrogen-doped carbon foams decorated with zinc nanodots originating from carbothermal reaction (Zn@NCFs).

The X-ray diffraction (XRD) results of Zn@NCFs and NCFs are given in Fig. 2a. Zn@NCFs and NCFs all show only (002) and (101) carbon peaks at $2\theta = 26°$ and 44° without clear zinc peaks, certifying that the carbon phase is amorphous and zinc may be homogeneously distributed in the carbon matrix after carbonization [28]. In the Raman spectroscopy of Zn@NCFs and NCFs (Fig. 2b), the D-band centered at 1350 cm^{-1} is related to distribution and defects of hybridized carbon rings (sp^2) [29]. The G-band centered at around 1596 cm^{-1} is related to stretching of sp^2 hybridized carbon [28]. It is widely accepted that the ratio of I_D/I_G is proportional to the number of sp^2 hybridized carbon rings [29,30]. The ratio I_D/I_G of Zn@NCFs is about 2.5, lower than that ($I_D/I_G = 3.2$) of NCFs matrix, indicating that Zn@NCFs possess a more disordered structure, which probably originates from the presence of zinc. In order to analyze the porous structure of Zn@NCFs, N_2 (−196 °C) physisorption experiments were performed (Figs. 2c and d). The results are consistent with typical type I isotherm, which show the existence of a small number of mesopores (specific surface area (SSA), 242.9 m^2/g).

X-ray photo-electron spectroscopy (XPS) was conducted to identify the distribution and chemical states of different elements (Fig. 3). In the survey XPS spectra of Zn@NCFs, the two peaks at

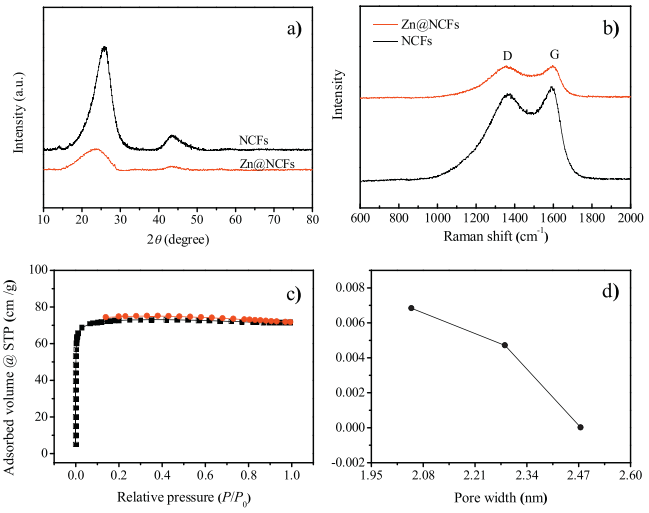

Fig. 2. (a) XRD patterns of Zn@NCF and NCFs. (b) Raman spectra of NCFs and Zn@NCFs. (c) N_2 physisorption isotherms and (d) pore-size distribution curve of Zn@NCFs.

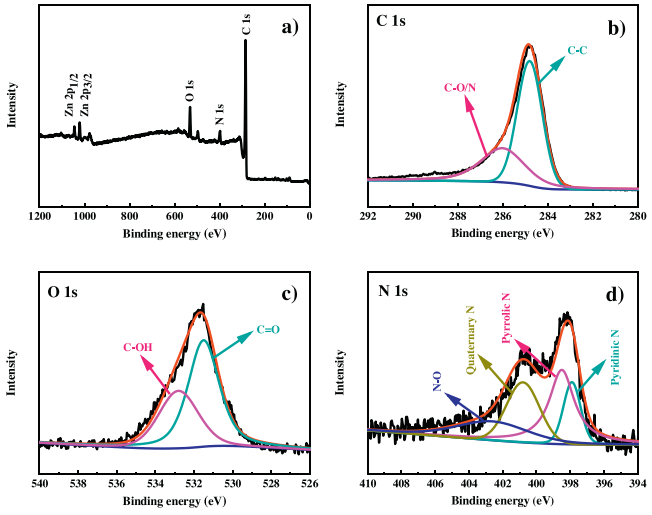

Fig. 3. (a) The XPS survey spectra and high-resolution (b) C 1s, (c) O 1s and (d) N 1s XPS spectra of Zn@NCFs.

284.8 and 286.1 eV can be attributed to C−C and C−O/C−N in high-resolution C 1s spectra respectively [31]. The peaks at 397.9, 398.5, 400.8 and 402.6 eV in high-resolution N 1s spectra are assigned to pyridinic N, pyrrolic N, quarternary N and N−O species

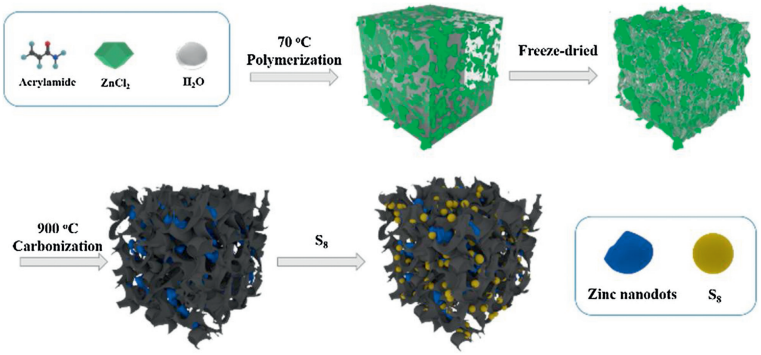

Fig. 1. Schematic description of the synthesis of nitrogen-doped carbon foams decorated with zinc nanodots (Zn@NCFs) and the fabrication of Zn@NCFs/S cathode by the chemisorption of S_8.

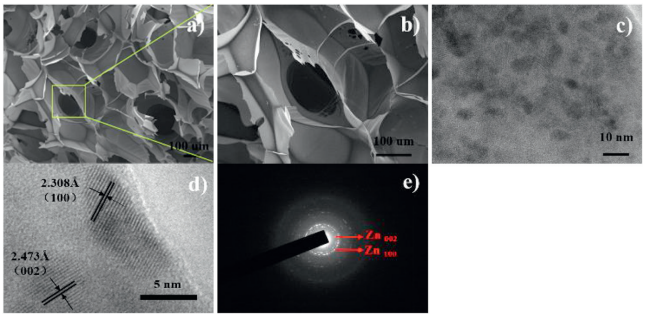

Fig. 4. (a, b) SEM micrographs, (c, d) HRTEM images and (e) selected area electron diffraction (SAED) pattern of Zn@NCFs.

correspondingly due to nitrogen doping [32,33]. The two peaks located at 531.5 and 532.8 eV in high-resolution O 1s spectra correspond to C=O and C−OH species [28].

Scanning electron microscopy (SEM) are conducted to gain an insight into the morphology of Zn@NCFs and the results are given in Figs. 4a and b. Zn@NCFs have a loose foam structure with apparent macropores, which is because $ZnCl_2$ impregnated in PAM hydrogels serves as chemical activation agent in carbonization. The microstructure of Zn@NCFs is further studied by transmission electron microscopy (TEM). The morphology clearly shows uniformly-distributed zinc nanodots with diameters smaller than 10 nm (Fig. 4c) [28]. The micrograph of high-resolution TEM (HRTEM) shows parallel lattice fringes with spacings of 2.308 and 2.437 Å, which are attributed to the zinc metal (100) and (002) crystal faces. The selected area electron diffraction (SAED) patterns in Fig. 4e display diffraction rings attributed to the Zn (100) and (002) in-plane reflections, which prove the polycrystals of zinc nanodots. In addition, 100 zinc nanodots in Fig. S2 (Supporting information) are measured, showing that the zinc nanodots have an average diameter of 5.6 nm.

Zn@NCFs/S hybrid material was prepared by a typical melt-diffusion process as reported [34]. Briefly, a mixture of Zn@NCFs and sublimed sulfur powder at a weight ratio of 4:6 was hand grounded. The product was added into an autoclave with stainless steel followed by being heated at 155 °C for 12 h. Zn@NCFs/S and NCFs/S composites were characterized by XRD to gain an insight into the different forms of sulfur species (Fig. 5a). The sharp peak corresponding to the sulfur phase indicates its existence in a crystalline state. The main strong peaks at 164.0 and 165.2 eV can be attributed to S $2p_{3/2}$ and S $2p_{1/2}$ (Fig. 5b) [10]. The peak located at 168.8 eV is ascribed to the sulfate which is formed due to oxidation of sulfur in air [14], while the energy peak at around 162.0 eV can be contributed to the Zn—S bonding between zinc metal and sulfur [34].

UV–vis spectroscopy was used to study the adsorption of polysulfides further (Fig. S3 in Supporting information). Strong absorption of fresh Li_2S_6 solution between 400 nm and 500 nm can be clearly seen, which is consistent with the literature [35]. The solutions with NCFs and Zn@NCFs exhibit lower absorbance between 400 nm and 500 nm in comparison to the control sample (Li_2S_6 solution) due to the physical absorption of porous matrix and chemisorption of heteroatoms (N, O). It is specially noted that Zn@NCFs has the lowest absorbance of polysulfides, which arises from the extra contribution from the strong interaction of zinc nanodots with polysulfides. Thermogravimetric analysis (TGA) was conducted to determine sulfur content (≈ 60 wt%) (Fig. S4 in Supporting information). Elemental mapping of Zn@NCFs (Fig. S5 in Supporting information) and NCFs/S (Fig. S6 in Supporting information) was carried out by energy-dispersive X-ray spectroscopy (EDS), which not only indicates the presence of C, N, O, Zn and S, but also illustrates a uniform distribution of N and Zn on carbon foams. The structural features described above are believed to facilitate the electrochemical performance of the Zn@NCFs/S cathode.

The initial three CV curves of Zn@NCFs/S and NCFs/S conducted at a scan rate of 0.1 mV/s are shown in Fig. 6a and Fig. S7 (Supporting information) between 1.5 V and 3.0 V. It can be seen that there are two typical cathodic peaks and an anode peak in all cathodes, which is related to the reaction between sulfur and Li_2S/Li_2S_2 [36]. The cathodic peaks can be assignedto the electrochemical reactions: $S_8 \rightarrow Li_2S_x$ $(4 \leq x \leq 8)$ and $Li_2S_x \rightarrow Li_2S_2/Li_2S$. The anodic peak represents the conversion of Li_2S_x $(4 \leq x \leq 8)$ from lithium sulfides (Li_2S_2/Li_2S) and then to sulfur. The potential differences of the cathodic and anode peaks for the Zn@NCFs/S cathode are smaller than those of the NCFs/S, showing smaller polarization of the Zn@NCFs/S electrode. There is one plateau (∼2.4 V) in the charge profile, while two clear discharge platforms (∼2.3 and 2.0 V) can be seen in the discharge profile (Fig. 6b and Fig. S8 in Supporting information). These results are in line with previously-reported carbon-based cathodes in Li-S battery [37].

The rate performances of these cathodes are evaluated at various C rates. As can be seen from Fig. 6c, the capacities of the NCFs/S cathode are only 916, 640, 544, 470 and 367 mAh/g when the rates are at 0.2 C, 0.5 C, 1 C, 2 C and 5 C (1 C = 1675 mAh/g), respectively. In contrast, the Zn@NCFs/S cathode demonstrates capacities as high as 1065, 737, 630, 582 and 528 mAh/g under identical conditions. The cycle stability of the Zn@NCFs/S and NCFs/S cathodes at a high rate (2 C, 1 C = 1675 mA/g) is compared in Fig. 6d. The NCFs/S cathode exhibits a dramatic decline from 815 mAh/g in the initial cycle to 342 mAh/g after 100 cycles, representing a capacity decay of 0.580% per cycle. In comparison, the Zn@NCFs/S cathode still has a high capacity (505 mAh/g) at 2 C after 100 cycles (first discharge capacity: 963 mAh/g), which corresponds to a lower capacity decay (only 0.476%). This can be understood when taking into account of the strong interaction between polysulfides and zinc nanodots, which contributes to better polysulfides confinement, and thus, better cycle stability.

In addition, electrochemical impedance spectroscopy (EIS) was conducted to investigate the internal and charge transfer

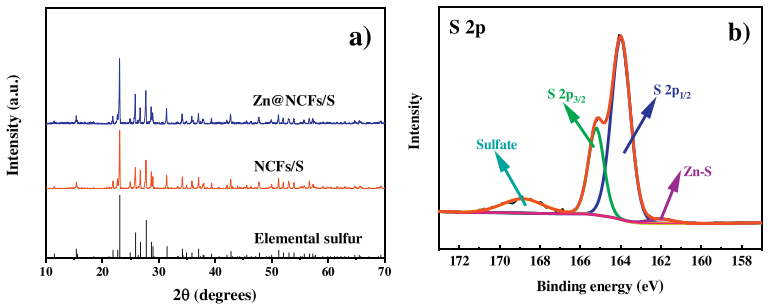

Fig. 5. (a) XRD patterns of NCFs/S and Zn@NCFs/S cathodes and (b) S 2p XPS spectra of Zn@NCFs/S.

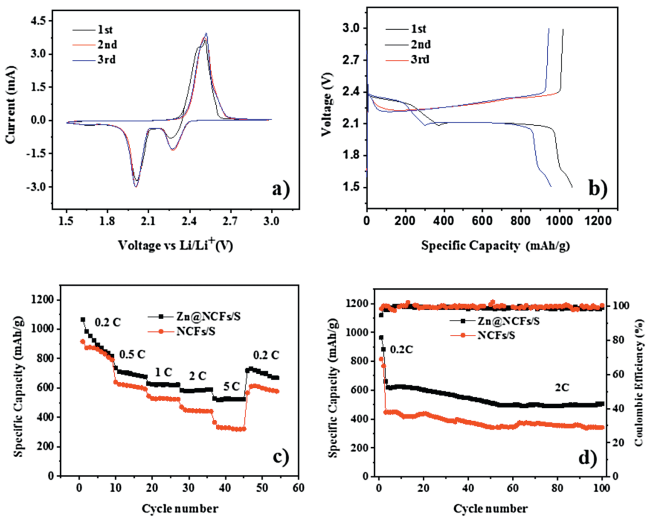

Fig. 6. (a) Cyclic voltammetry (CV) curves of the Zn@NCFs/S between 1.5 C and 3.0 V at 0.1 mV/s. (b) Initial three charge/discharge curves of the Zn@NCFs/S during charge/discharge process (0.2 C). (c) Rate capability test results of Zn@NCFs/S and NCFs/S batteries. (d) Cycle behaviors at 2 C of Zn@NCFs/S and NCFs/S cathodes (1 C = 1675 mA/g).

resistance of the Li-S cells with NCFs/S and Zn@NCFs/S cathodes (Figs. S9a and b in Supporting information). The Nyquist plots for the NCFs/S and Zn@NCFs/S cathodes consist of two semicircles recessed inward (high-frequency region) and a sloped line (low-frequency range).The main parameter is the diameter of the second depressed semicircle related to charge-transfer resistance R_{ct}, which can be seen in the equivalent circuit model (Fig. S9c in Supporting information). Compared with typical Al-based cathodes, the R_{ct} values of the cells with NCFs/S and Zn@NCFs/S cathodes are smaller [38]. This can be explained by the lower resistance and faster charge transfer of NCFs/S and Zn@NCFs/S cathodes in battery testing. The R_{ct} value of Zn@NCFs/S cathode is even smaller than that of NCFs/S cathode. After 20 cycles, the curve of Zn@NCFs/S still has a high degree of coincidence, indicating that it has higher interfacial stability, which is because that zinc nanodots can provide more active sites at the interface and trap polysulfides.

In conclusion, we have proposed a novel and simple approach to hierarchically porous nitrogen-doped carbon foams decorated with zinc nanodots, which can serve as sulfur hosts. The Zn@NCFs/S cathode displays a strikingly high cycle capacity (505 mAh/g, 2 C) after 100 cycles and excellent rate performance, which outweighs the test results of NCFs/S cathode. This should be mainly ascribed to strong chemical bond between zinc nanodots and polysulfides in addition to physical absorption of porous structure. We believe our work could provide a new choice to develop cathode electrodes with excellent properties for Li-S batteries.

Declaration of competing interest

The authors declare that they have no known competing financial interests or personal relationships that could have appeared to influence the work reported in this paper.

Appendix A. Supplementary data

Supplementary material related to this article can be found, in the online version, at doi:https://doi.org/10.1016/j.cclet.2021.02.027.

References

[1] Q. Pang, X. Liang, C.Y. Kwok, L.F. Nazar, Nat. Energy 1 (2019) 16132.
[2] T. Tao, S. Lu, Y. Fan, et al., Adv. Mater. 29 (2017) 1700524.
[3] Y. Wang, X. Huang, S. Zhang, Y. Hou, Small Method. 2 (2018) 1700345.
[4] L. Borchardt, M. Oschatz, S. Kaskel, Chemistry 22 (2016) 7324–7351.
[5] G.D. Park, Y.C. Kang, Appl. Surf. Sci. 495 (2019) 143637.
[6] T. Ma, M. Liu, T. Huang, A. Yu, J. Power Sources 398 (2018) 75–82.
[7] K. Chen, J. Cao, Q. Lu, et al., Nano Res. 11 (2018) 1345–1357.
[8] D.B. Babu, K. Ramesha, Carbon 144 (2019) 582–590.
[9] Q. Sun, B. He, X.Q. Zhang, A.H. Lu, ACS Nano 9 (2015) 8504–8513.
[10] W. Kang, L. Fan, N. Deng, et al., Chem. Eng. J. 333 (2018) 185–190.
[11] Q. Lu, X. Wang, J. Cao, et al., Energy Storage Mater. 8 (2017) 77–84.
[12] L. Ma, H.L. Zhuang, S. Wei, et al., ACS Nano 10 (2016) 1050–1059.
[13] H. Li, Z. Wang, Y. Zhang, et al., Russian J. Appl. Chem. 89 (2016) 1336–1340.
[14] C. Fu, M.B. Oviedo, Y. Zhu, et al., ACS Nano 12 (2018) 9775–9784.
[15] W. Yang, W. Yang, A. Song, G. Sun, G. Shao, Nanoscale 10 (2018) 816–824.
[16] Z. Zhang, L.L. Kong, S. Liu, G.R. Li, X.P. Gao, Adv. Energy Mater. 7 (2017) 1602543.
[17] Y.Z. Zhang, Z. Zhang, S. Liu, G.R. Li, X.P. Gao, ACS Appl. Mater. Interfaces 10 (2018) 8749–8757.
[18] S. Ma, L. Wang, Y. Wang, et al., Carbon 143 (2019) 878–889.
[19] H. Ding, Q. Zhang, Z. Liu, et al., Electrochim. Acta 284 (2018) 314–320.
[20] Y. Yang, H. Xu, S. Wang, et al., Electrochim. Acta 297 (2019) 641–649.
[21] Y. Wang, Y. Lu, R. Luo, et al., Ceramics Int. 44 (2018) 16265–16272.
[22] K. Lu, H. Zhang, S. Gao, et al., Adv. Funct. Mater. 29 (2019) 1807309.
[23] P. Rajkumar, K. Diwakar, G. Radhika, et al., Vacuum 161 (2019) 37–48.
[24] F. Luna-Lama, C. Hernández-Rentero, A. Caballero, J. Morales, Electrochim. Acta 292 (2018) 522–531.
[25] X. Feng, Q. Wang, R. Li, H. Li, Appl. Surf. Sci. 478 (2019) 341–346.
[26] Q. Liu, Q. Jiang, L. Jiang, J. Peng, Y. Gao, Appl. Surf. Sci. 462 (2018) 393–398.
[27] J. Li, S. Chen, N. Yang, et al., Angew. Chem. Int. Ed. 58 (2019) 7035–7039.
[28] R. Yan, M. Antonietti, M. Oschatz, Adv. Energy Mater. 8 (2018) 1800026.
[29] M. Pawlyta, J.N. Rouzaud, S. Duber, Carbon 84 (2015) 479–490.
[30] S. Osswald, J. Chmiola, Y. Gogotsi, Carbon 50 (2012) 4880–4886.
[31] G. Liu, Z. Liu, J. Li, et al., Carbon 137 (2018) 68–77.
[32] J. Li, Z. Li, J. Tong, C. Xia, F. Li, RSC Adv. 5 (2015) 70010–70016.
[33] J. Zhang, Z. Zhao, Z. Xia, L. Dai, Nat. Nanotechnol. 10 (2015) 444–452.
[34] F. Teng, Q. Liu, H. Zeng, J. Colloid Interface Sci. 368 (2012) 512–520.
[35] D. Maccariello, A. Al Taleb, F. Calleja, et al., Nano Lett. 16 (2016) 2–7.
[36] M.D. Patel, E. Cha, C. Kang, B. Gwalani, W. Choi, Carbon 118 (2017) 120–126.
[37] L. Qie, A. Manthiram, Adv. Mater. 27 (2015) 1694–1700.
[38] R. Fang, S. Zhao, P. Hou, et al., Adv. Mater. 28 (2016) 3374–3382.